Biochemistry

Article

Cite This: Biochemistry 2018, 57, 6669−6678

pubs.acs.org/biochemistry

Salvaging the Thermodynamic Destabilization of Interface Histidine in Transmembrane β-Barrels

Bharat Ramasubramanian Iyer, Pallavi Vijay Vetal, Henna Noordeen, Punit Zadafiya, and Radhakrishnan Mahalakshmi*

Molecular Biophysics Laboratory, Department of Biological Sciences, Indian Institute of Science Education and Research, Bhopal 462066, India

Supporting Information

ABSTRACT: The ability of histidine to participate in a wide range of stabilizing polar interactions preferentially populates this residue in functionally important sites of proteins. Histidine possesses an amphiphilic and electrostatic nature that is essential for amino acids residing at membrane interfaces. However, the frequency of occurrence of histidine at membrane interfaces, particularly transmembrane β-barrels, is lower than those of other aromatic residues. Here, we carry out comprehensive energetic measurements using equilibrium folding of the outer membrane enzyme PagP to address the contribution of a C-terminal interface histidine to barrel stability. We show that placing histidine at the C-terminus universally destabilizes PagP by 4.0−8.0 kcal mol^{-1} irrespective of the neighboring residue. Spectroscopic and electrophoretic measurements indicate that the altered stability may arise from a loss of barrel compaction. Isoleucine, methionine, and valine salvage this destabilization marginally (in addition to tyrosine, which shows an exceptionally high folding free energy value), when placed at the penultimate position, at the expense of an altered folding pathway. Double-mutant cycle analysis indicates that the coupling energy between the terminal and penultimate residues in PagP-X^{160}H^{161} increases when the level of intrinsic destabilization by the terminal H^{161} is high. Our observations that neighboring residues cannot salvage the energetic destabilization of histidine may explain why histidine is less abundant at membrane interfaces.

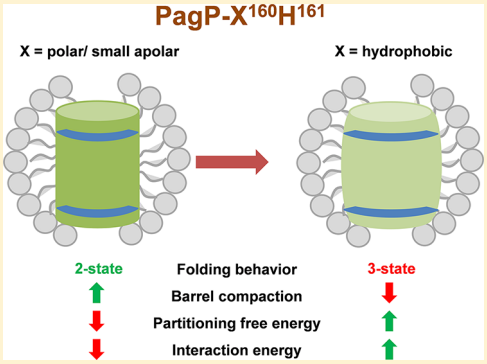

Histidine is the most versatile amino acid, because of its unique structural characteristics and its ability to participate in a wide range of intermolecular interactions.[1,2] Conventionally, the His side chain is considered polar in nature, with the ability to attain a positive charge dictated by the pH of the environment. Additionally, although the aromaticity of the side chain is low, His is classified as an aromatic residue because of its conjugation system. Indeed, the His side chain is known to stabilize proteins through long-range aromatic interactions with neighboring residues.[1,3−6] Despite the amphiphilic nature of its side chain, His occurs with a reasonably low frequency at the water−lipid interface of membrane proteins.[7] Hydrophobicity scales for membrane proteins show a favorable contribution for His when it is positioned between the interface and the bilayer midplane.[7,8] The probability of finding His along the membrane normal decreases as we move closer to the interface or the middle of the membrane.[8]

Membrane proteins themselves possess a unique architecture, with hydrophobic functional groups presented to the surrounding lipid environment and a polar surface interacting with the aqueous milieu.[7,9,10] Within membrane proteins, His is known to play a key role in promoting protein−lipid interactions, particularly at the interface, by means of interaction between the positively charged imidazole side chain and the negatively charged headgroup of lipid moieties,[11−14] yet the frequency of occurrence of His in transmembrane helices is lower than those of Phe, Tyr, and Trp; the frequency is decreased further in bacterial outer membrane proteins (OMPs).[7] A reasonable assumption based on existing hydrophobicity scales[15−18] would be that His is thermodynamically less favored than the other aromatic residues. Hence, it is interesting to examine whether the partitioning of histidine at the water−lipid interface could be made energetically favorable by providing an environment that does not favor its polar nature. By performing free energy measurements under alkaline conditions (pH 9.5), we can alter the ionized state of the His side chain (pK_a of 6.0) and render it as an aromatic residue as opposed to a polar molecule.

Transmembrane β-barrel proteins (OMPs) of the bacterial outer membrane serve as excellent model systems for deducing the partitioning free energy of each amino acid side chain, from water to the bilayer.[17,19−22] They possess a C-terminal β-signal motif with an evolutionarily conserved Aro1-Xxx2-Aro3 sequence (Aro = aromatic; Xxx = small polar residue). In the case of the outer membrane protein PagP (PhoPQ-

Received: July 31, 2018
Revised: September 18, 2018
Published: October 4, 2018

DOI: 10.1021/acs.biochem.8b00805
Biochemistry 2018, 57, 6669−6678

activated gene P), which has a total chain length of 161 residues, this β-signal can be represented as Phe^{159}-Gln^{160}-Phe^{161}. Aro3 is the terminal residue and is positioned at the membrane interface;[23] here, Phe is preferred (as observed in wild-type PagP), while Tyr and Trp are also observed.[23−28] Xxx^{160} is the penultimate residue, with the side chain (Gln^{160} in PagP) oriented toward the barrel interior. His is observed at the Aro1 position, which is a lipid-facing site (up to 57% occurrence in the case of β-proteobacteria), and at other positions across the strand as well as in the loop regions of transmembrane barrels.[7,8] Interestingly, His is conspicuously absent at Aro3.[28] Indeed, the abundance of His is low at the interface region in most OMPs.[7,28] However, a detailed thermodynamic study that addresses this feature is currently lacking. Aro3 of the β-signal motif serves as an excellent site for studying the energetic implications of an interface His for two reasons. (i) Unlike the interface residues in the other β-strands, intrinsic strand fraying is observed in the vicinity of the β-signal in folded OMPs. Strand registry (or fraying) would amplify the thermodynamics sufficiently to obtain a reliable measure of those mutants that are indeed highly stabilizing or destabilizing for OMPs. (ii) The thermodynamics of the C-terminal Aro-Xxx-Aro motif has been examined previously for the bacterial OMP PagP[22] and would serve as a useful reference for addressing the thermodynamic contribution of His^{161}. Biophysical studies suggest that the C-terminal β-signal motif may also have a crucial role in uncatalyzed β-barrel folding,[20,29,30] which involves a combination of both protein-facing and lipid-facing residues. Hence, we used the β-signal motif to ask whether there is a thermodynamic factor that excludes His at the interface and if such a destabilization can be rescued by optimal energetic contributions of the penultimate residue.

Here, we examine the energetic contribution of His as an aromatic polar substituent at the bilayer interface. We use the eight-stranded OMP enzyme PagP as our model, because of the ability of PagP to exhibit reversible folding under an array of experimental conditions.[20,22] We observe that replacement of Phe with His at the C-terminal interface thermodynamically destabilizes the β-barrel by preventing PagP from forming a compact structure. Furthermore, it is known that noncovalent interactions established by the protein-facing interface residue at positon 160 (Gln in wild-type PagP) in the interior of the PagP barrel can be crucial to the stabilization of the folded structure.[20,22] Hence, we studied the importance of the penultimate protein-facing interface residue X^{160} in PagP-H^{161} (as opposed to F^{161}) for strand registry, barrel compaction, and PagP oligomerization. We find that X^{160} can conditionally salvage this H^{161}-mediated destabilization of PagP. Data derived from the double-mutant cycle analysis suggest that the interaction energy between the terminal and penultimate residues is a function of the intrinsic destabilization caused by histidine incorporation. Our results provide thermodynamic insight into the evolutionary preference of specific residues in the OMP primary sequence and the physical principles that govern the folding and stability of membrane proteins.

EXPERIMENTAL METHODS

Cloning and Protein Expression. The cloning of the *pagP* wild-type (WT) gene was performed in the pET3a vector between the NdeI and BamHI sites. A library of point mutations was created using a modified site-directed mutagenesis protocol,[31] where the terminal Phe was mutated first to His, followed by Gln → Xxx (where Xxx = other 19 amino acids). Sanger sequencing was used to confirm the mutant sequence. *Escherichia coli* BL21 (DE3) competent cells were transformed with the plasmid and used for protein production. Each protein was overexpressed as inclusion bodies after induction with 1 mM isopropyl β-D-thiogalactopyranoside and processed to ∼95% purity using reported protocols.[22]

Unfolded PagP Stock Preparation for Equilibrium Folding Experiments. The unfolded protein stock was prepared by solubilizing the protein in 8 M urea prepared in 20 mM Tris-HCl (pH 9.5). After thorough mixing and centrifugation at 16600*g* for 1 h at 25 °C, the supernatant was collected. The concentration of the protein stock was decreased to ∼0.3 mM using the absorbance at 280 nm (molar extinction coefficient of 82390 M^{-1} cm^{-1}). This unfolded protein was diluted 10-fold in a solution of 100 mM DPC (*n*-dodecylphosphocholine) and 8 M GdnHCl (guanidine hydrochloride) in 20 mM Tris-HCl (pH 9.5).[22] The mixture was centrifuged for 1 h at 16600*g*, and the supernatant was collected.

Equilibrium Folding Experiments Using Steady State Fluorescence. For equilibrium folding measurements, the unfolded stock protein [30 μM PagP in 100 mM DPC, 20 mM Tris-HCl (pH 9.5), and 8 M GdnHCl] was diluted 10-fold in various GdnHCl concentrations ranging from ∼0.7 to ∼6.6 M, in 0.1 M increments. This resulted in a final protein concentration of 3 μM and a final DPC concentration of 10 mM, corresponding to a DPR (detergent-to-protein ratio) of ∼3300:1. Samples were incubated at 25 °C, and fluorescence measurements were taken on a SpectraMax M5 microplate reader. The progress of the reaction was monitored using intrinsic tryptophan fluorescence using a $\lambda_{ex\text{-}max}$ of 295 nm and a λ_{em} of 320−400 nm. Equilibrium was reached within 24 h.

Analysis of Equilibrium Folding Data. All data obtained from the fluorescence experiments were analyzed using SigmaPlot version 11.0. We used the 48 h time point data for calculation of thermodynamic parameters. Fluorescence intensities obtained from chemical denaturation were converted to fraction unfolded (f_U) using eq 1, as reported previously.[22]

$$f_U = \frac{y_O - (y_N + m_N[D])}{y_U + m_U[D] - (y_N + m_N[D])} \quad (1)$$

where y_O is the observed fluorescence at GdnHCl concentration [D] whereas y_N, m_N, y_U, and m_U are intercepts and slopes of the pre- and post-transition baselines, respectively.

We were able to explain the folding transitions for several of the mutants using the two-state linear extrapolation model (eq 2).[32]

$$f_U = \frac{\exp[-(\Delta G^\circ + m[D])/RT]}{1 + \exp[-(\Delta G^\circ + m[D])/RT]} \quad (2)$$

According to this model, the protein folds from the unfolded (U) to the native (N) state in a cooperative manner without a detectable intermediate. We obtained the thermodynamic parameters ΔG° ($\Delta G_F^{\circ,H_2O}$, Gibbs folding free energy) and *m* value (change in accessible surface area between U and N states) of folding from the fits of the data to eq 2. The midpoint of chemical denaturation (C_m) was derived as $C_m = \Delta G^\circ/m$.

DOI: 10.1021/acs.biochem.8b00805
Biochemistry 2018, 57, 6669−6678

The folding transition of some mutants could be explained only using a three-state model (eq 3), because of the occurrence of an intermediate (I).[22] Here, we obtained ΔG°_1, ΔG°_2, and their corresponding m_1 and m_2 values for the change in free energy from the first (U → I) and second (I → N) transitions, respectively.

$$f_U = \left\{ y_F + m_F[D] + \left[\exp\left(-\frac{\Delta G^{\circ}_1 + m_1[D]}{RT} \right) (y_I + m_I[D]) \right] + \left[\exp\left(-\frac{\Delta G^{\circ}_1 + m_1[D]}{RT} \right) \exp\left(-\frac{\Delta G^{\circ}_2 + m_2[D]}{RT} \right) (y_U + m_U[D]) \right] \right\} \Big/ \left[1 + \exp\left(-\frac{\Delta G^{\circ}_1 + m_1[D]}{RT} \right) + \exp\left(-\frac{\Delta G^{\circ}_1 + m_1[D]}{RT} \right) \exp\left(-\frac{\Delta G^{\circ}_2 + m_2[D]}{RT} \right) \right] \quad (3)$$

Double-Mutant Cycle. We calculated the interaction energy between the protein-facing (160th) and lipid-facing (161st) interface residues using the double-mutant cycle.[33] The difference between the folding free energies of the wild-type and mutant proteins ($\Delta\Delta G^0$) was calculated using eq 4.

$$\Delta\Delta G^{\circ} = \Delta G^{\circ}_{WT} - \Delta G^{\circ}_{mut} \quad (4)$$

For the double-mutant cycle analysis, we utilized the previously reported folding free energy values of the PagP-X^{160} library of mutants[22] and computed the interaction energy (ΔG_{int}) between residues Q^{160} and F^{161} using eq 5.

$$\Delta G_{int} = \Delta\Delta G^{\circ}_{Q-X} + \Delta\Delta G^{\circ}_{F-H} - \Delta\Delta G^{\circ}_{Q-X,F-H} \quad (5)$$

where the amino acids that were mutated have been indicated by their single-letter codes in subscript and X represents any amino acid.

Electrophoretic Mobility, Proteolysis, and Circular Dichroism (CD) Measurements. Direct folding of PagP in DPC micelles was performed using the heat shock method described previously.[34] Briefly, PagP denatured in 8.0 M urea was diluted 10-fold into the folding mixture [100 mM DPC in 20 mM Tris-HCl (pH 9.5)] prechilled to 4 °C. A heat shock at 70 °C was administered for 3 min.[22,34] The sample was cooled immediately to 4 °C and incubated overnight. The next day, samples were centrifuged at 16600*g* for 1 h to remove any trace amounts of protein aggregates. Folded protein was checked for soluble aggregates on an ultraviolet (UV) spectrophotometer by monitoring the scattering between 300 and 340 nm. The final stock contained ∼15 μM PagP in 50 mM DPC and 20 mM Tris-HCl (pH 9.5), which corresponded to a DPR of ∼3300:1. We also monitored the folding of the samples electrophoretically, using cold sodium dodecyl sulfate−polyacrylamide gel electrophoresis (SDS−PAGE).[22,34,35] The electrophoretic mobility shift of this folded protein stock was quantified using densitometry analysis. The folding efficiency was further examined by the protease protection assay. Pulse proteolysis using proteinase K (PK) was carried out using minor modifications of reported protocols.[22]

Far-UV CD wavelength scans of folded PagP were obtained using a quartz cuvette with a 1 mm path length. The data were recorded at 5 °C, between 205 and 260 nm in 1 nm increments. The scans were averaged over three accumulations, corrected for buffer contributions, smoothed, and represented as raw ellipticity values.

RESULTS

Histidine at the C-Terminal Lipid-Facing Interface Destabilizes PagP. The eight-stranded β-barrel, PagP, can be readily folded *in vitro* into an array of membrane mimetics ranging from detergent micelles to lipidic vesicles.[20,22,36] We have previously shown that the reversible folding equilibrium of PagP from the unfolded state can be achieved using guanidine hydrochloride as the denaturant and DPC micelles as the membrane mimetic.[22] For this study, we first mutated the terminal F^{161} to H^{161} (Figure 1A). It must be noted here that Phe is highly conserved as the C-terminal residue in most OMPs.[23−25,28] Thereafter, we generated a library of PagP-$X^{160}H$ mutants (where X^{160} represents any amino acid) through mutagenesis. We verified that all the mutants were folded using spectroscopic parameters, an electrophoretic mobility shift assay, and resistance to proteolysis (details are in the Supporting Information and in the sections below). We confirmed that all mutants exhibited path independence (Figures S1 and S2), allowing us to derive the equilibrium thermodynamic parameters for each mutant.

We determined the Gibbs free energy ΔG° ($\Delta G_F^{o,H_2O}$, equilibrium free energy of folding), *m* value, and C_m for each PagP mutant. Here, the folding transitions of a majority of the PagP-$X^{160}H$ mutants could be described using a two-state model between the unfolded (U) and native (N) states, whereas others required a three-state model involving an intermediate (I) to derive the total ΔG° of folding (Figure 1B, Figure S3, and Table S1). The $F^{161} \rightarrow H^{161}$ mutation in PagP causes destabilization of the barrel by ∼4.3 kcal mol^{-1}. In addition, we find that a majority of the PagP-$X^{160}H$ mutants are less stable than wild-type PagP (Figure 1C), suggesting that the presence of a C-terminal His at position 161 causes a significant destabilizing effect on PagP. This destabilization is rescued marginally (except in the case of Tyr where the mutant is highly stabilized) when hydrophobic residues (Tyr > Met > Ile > Val > Leu) are placed at the penultimate position. The histidine side chain is uncharged at our experimental pH of 9.5, thereby rendering it an aromatic residue with a partial polar character. As described in an earlier report,[22] we could achieve reversible folding of PagP only at a pH of 9.5 in DPC micelles. Other buffer systems and pH conditions (including acidic pH) showed path dependence and depressed values for folding/unfolding cooperativity. Hence, we performed our studies at pH 9.5. By comparing the data with our previous analysis of PagP energetics,[22] we find that PagP-WT is destabilized to a similar extent by His and Trp (ΔG° difference of ∼1.5 kcal mol^{-1} between PagP-QH and -QW). A recent study of the anchoring role of Trp at membrane interfaces[37] highlights the similarity between Trp and His at protein sites where the hydrophobicity or polarity of the side chain (as opposed to the aromatic nature) dictates the stabilizing interactions. Essentially, aromatic residues such as Trp and His, with electrostatic aryl ring systems, appear to destabilize PagP significantly. Thus, the evolutionary selection of Phe (and, in some cases, Tyr) at the C-terminal interface of PagP appears to be a consequence of its hydrophobic nature.

The Nature of the Penultimate Residue Balances a High Stability with a Smooth Folding Landscape. Next, we calculated the energetic cost of incorporation of each residue with respect to alanine ($\Delta\Delta G^{\circ} = \Delta G^{\circ}_X - \Delta G^{\circ}_A$). Here, we find a unique distribution of amino acids, with hydrophobic residues such as Tyr and Ile at one end and

DOI: 10.1021/acs.biochem.8b00805
Biochemistry 2018, 57, 6669−6678

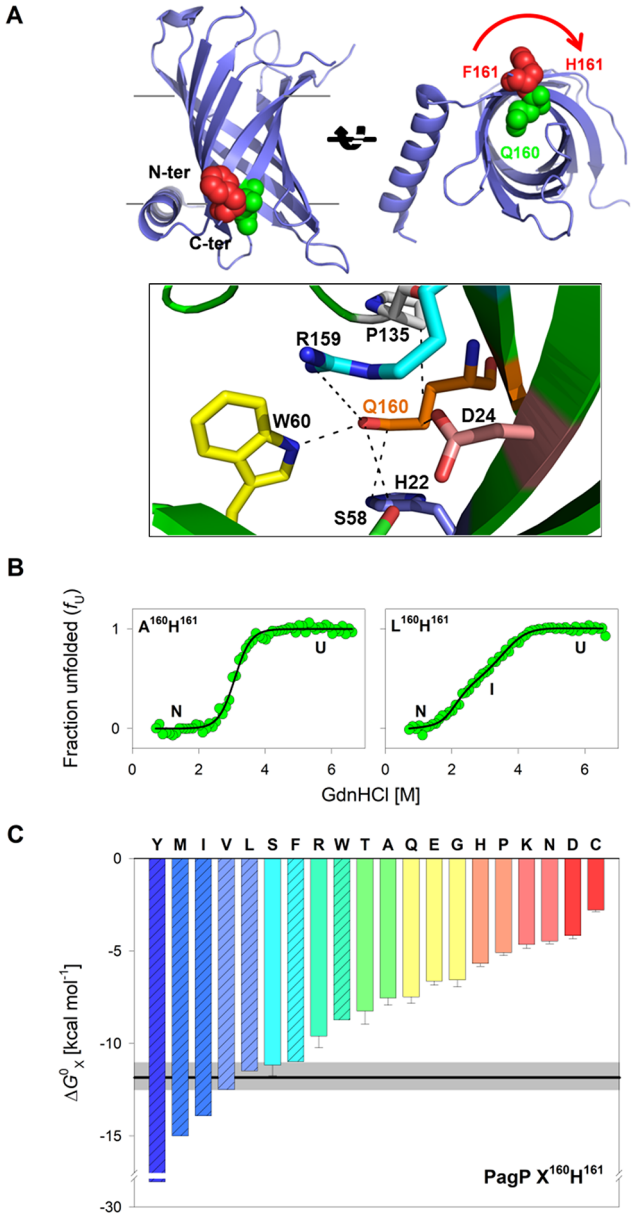

Figure 1. Histidine at the C-terminus of PagP is energetically destabilizing. (A) Schematic representations (top) of the eight-stranded transmembrane barrel PagP of *E. coli* (Protein Data Bank entry 3GP6) displaying the C-terminal (F^{161}, red spheres) and penultimate (Q^{160}, green spheres) residues that have been mutated in this study. The C-terminal Phe was replaced with His, and thereafter, the penultimate residue was mutated to generate the library of 20 PagP-$X^{160}H^{161}$ variants. Interaction map (bottom) of Q^{160} (orange) generated from the crystal structure of PagP (Protein Data Bank entry 3GP6) using PyMol.[38] The interaction network of all of the residues within 5 Å of the penultimate residue of PagP is annotated. (B) Normalized population of unfolded protein (f_U) measured from the fluorescence emission of the 12 intrinsic Trp residues of PagP at a $\lambda_{em\text{-}max}$ of 344 nm at increasing denaturant concentrations. Data for two representative mutants are shown (green spheres), fitted (solid line) to a two-state (left, PagP-AH) or three-state (right, PagP-LH) function, depending on the folding transition observed for each mutant (see Figure S3 for the complete data from the PagP-$X^{160}H^{161}$ library). (C) Equilibrium folding free energy values calculated for all 20 mutants of the PagP-$X^{160}H^{161}$ library. Histograms are colored from blue (most stable) to red (least stable). Error bars denote the goodness of fit of the fluorescence data. Amino acids are represented by their single-letter codes. ΔG° values of mutants showing three-state profiles are shown as a patterned fill in the histogram. The horizontal solid black line represents the ΔG° of PagP-WT (PagP-$Q^{160}F^{161}$), obtained from an earlier study, with the gray bar denoting the standard error derived for the free energy value.[22] With the exception of a few residues (Y, M, I, and V), all PagP-$X^{160}H^{161}$ mutants are less stable than PagP-WT.

charged residues such as Lys and Asp at the other (Figure 2). On the basis of the thermodynamic stability, it appears that

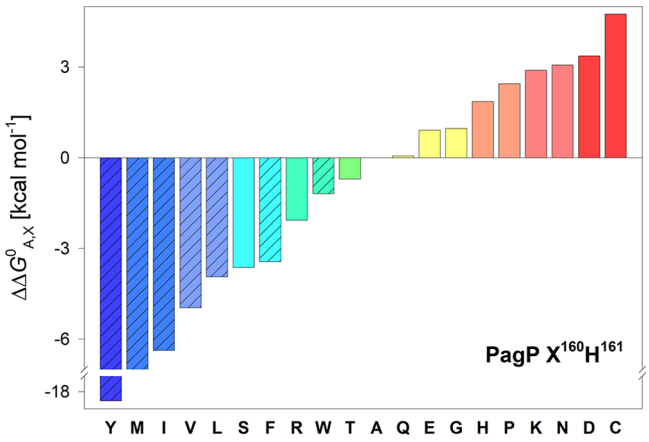

Figure 2. Folding free energies of the PagP-$X^{160}H^{161}$ mutants. Folding free energy values measured for all 20 residues at the protein-facing hydrophilic interface position, normalized with respect to alanine. The color code and histogram representation are retained from Figure 1.

hydrophobic amino acids with bulky side chains are energetically favorable at position 160. We reach a similar conclusion when we compare the folding free energy values with empirical parameters describing the change in the accessible surface area (ASA) for each amino acid[39] (Figure S4). Ser and Pro, however, are exceptions to this general trend. Although Ser possesses a polar side chain, the PagP-SH mutant is grouped with hydrophobic residues, while the apolar Pro has a $\Delta\Delta G^\circ$ similar to those of the hydrophilic amino acids. The stabilization observed for PagP-SH may be a consequence of better packing interactions provided by the Ser side chain, whereas the anomalous behavior of the proline mutant is a likely additive effect of the loss of hydrogen bonding ability as well as the constraints on the backbone ϕ. Cys is another interesting outlier, with a side chain structurally similar to Ser but a normalized folding free energy with respect to Ala of 4.75 ± 0.40 kcal mol^{-1}, the lowest among those of the 20 amino acid residues. We believe that the thiol group of cysteine may attain a negative charge (thiolate group) at our experimental pH and thereby cause repulsion with the D^{24} side chain [which is spatially proximal in folded PagP (Figure 1A)], causing destabilization of the barrel. Indeed, an earlier study of the active site mechanism of PagP[40] provides a precedent for the presence of a thiolate anion in the interior of the PagP barrel.

The observed distribution in our $\Delta\Delta G^\circ$ plot is unexpected, as position 160 faces the aqueous interior of the barrel and is likely to energetically favor polar and charged residues. Upon closer examination of the folding free energy scale, we find that seven of the nine mutations with high $\Delta\Delta G^\circ$ values enable PagP to undergo three-state folding with a prominent

DOI: 10.1021/acs.biochem.8b00805
Biochemistry 2018, 57, 6669−6678

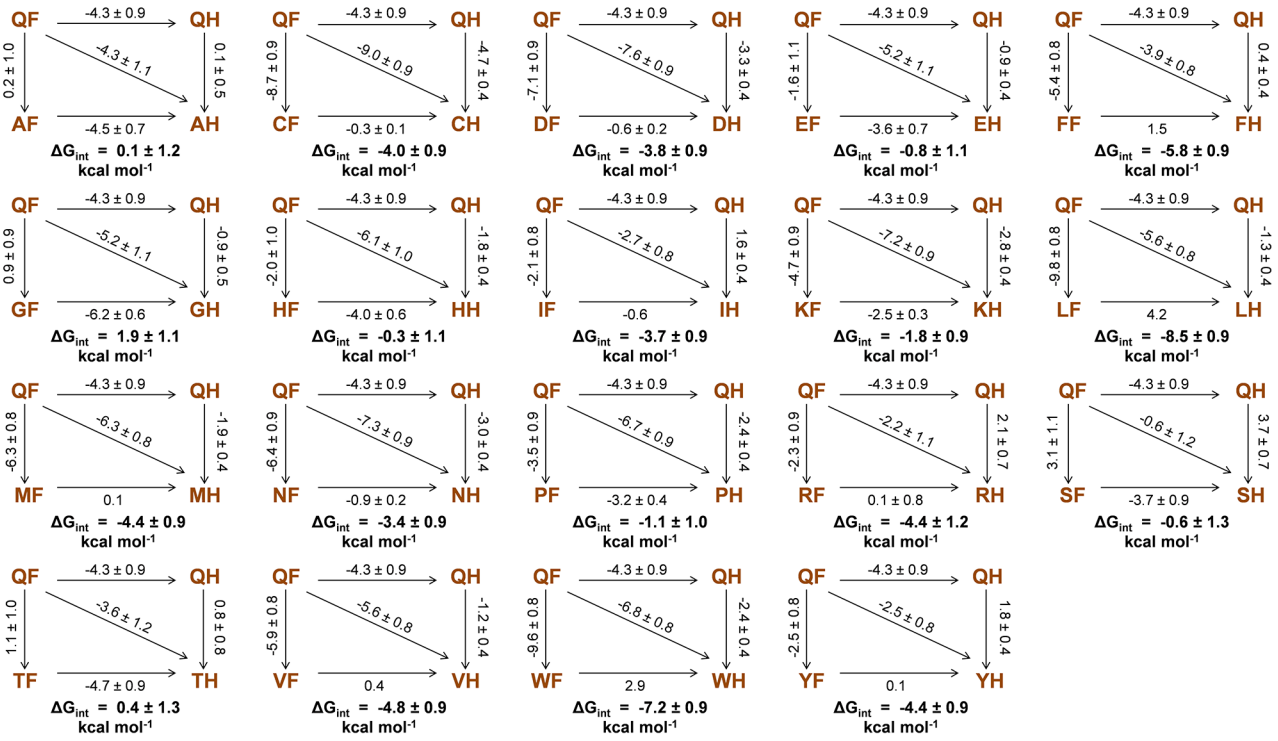

Figure 3. Double-mutant cycles for estimating the interaction energy between the side chains of the terminal and penultimate residues. Folding free energy values obtained from the equilibrium titrations were used to carry out the double-mutant cycle analysis to obtain the interaction energy (ΔG_{int}). The ΔG° for the PagP-$X^{160}F^{161}$ library was obtained from a previous report.[22] For the PagP-$X^{160}H^{161}$ mutants exhibiting three-state folding profiles (F, I, L, M, V, W, and Y), we used the $\Delta G^\circ_{U\rightarrow I}$ for the calculation (see Figure S8 for the calculation using $\Delta G^\circ_{U\rightarrow N}$). Mutants are named with single-letter codes for residues present at the two terminal positions. The free energy values and interaction energies are reported in units of kilocalories per mole. Errors in some cases are omitted because reliable error values could not be derived for the mutants describing three-state folding transitions.

equilibrium intermediate (histograms with patterned fill in Figure 2). The change in ASA obtained from the *m* value (ranging from 1.5 to 3.3 kcal mol^{-1} M^{-1} in most cases) indicates that the folding remains cooperative across nearly all the mutants. Hence, the mutation promotes the population of alternative folding pathways in PagP. As noted above, incorporation of a hydrophobic residue (such as Tyr, Met, or Ile) at the penultimate position (X^{160}) affects the folding landscape of the mutant, giving rise to the formation of a stable intermediate. Consequently, the local contacts established in this intermediate contribute to the calculated $\Delta\Delta G^\circ$ values with respect to alanine. To understand this phenomenon, we examine the spatial orientation of residue 160 and its interacting partners in the native structure of PagP (Figure 1A, bottom panel). We find that W^{60}, D^{24}, and H^{22} are potential interacting partners for Q^{160}. Q^{160} is also involved in the formation of a hydrogen bond with W^{60}. Polar residues such as Ser and Thr, which can maintain this hydrogen bonding network, demonstrate two-state folding profiles similar to that of wild-type PagP and retain free energy values similar to that of Q^{160} (present in wild-type PagP). Substitution of Q^{160} with hydrophobic residues gives rise to roughness in the PagP folding landscape and the likely formation of non-native interactions arising from molecular rearrangements required to accommodate bulky side chains in the interior of the PagP barrel.[22] The calculated $\Delta\Delta G^\circ$ is therefore unusually large for a single-residue mutation. We note here that partitioning free energy scales derived for lipid-facing interface sites (such as the Wimley–White interface scale)[41] may not apply to the molecular interactions taking place at the pore-facing X^{160} site of PagP. Unlike α-helices, residues in β-sheet structures can occlude greater nonpolar surface area,[42] also accounting for the differences in the calculated $\Delta\Delta G^\circ$. Another interesting observation is the difference in the $\Delta\Delta G^\circ$ values observed for the negatively charged residues: Glu and Asp. Replacing Q^{160} with D places the carboxyl side chain of D^{160} within 1.7 Å of D^{24} (Figure 1A, bottom panel), giving rise to possible charge–charge repulsion. Such unfavorable interactions are less pronounced in PagP-E^{160} or PagP-Q^{160} (PagP-WT).

For the equilibrium folding profiles of the subset of PagP-$X^{160}H$ mutants that show two distinct transitions (three-state folders), the total $\Delta G^\circ_{U\rightarrow N}$ can be separated into two individual values, $\Delta G^\circ_{U\rightarrow I}$ (change in ΔG° from U to I) and $\Delta G^\circ_{I\rightarrow N}$ (change in ΔG° from I to N). When we assess the energetic contribution of each residue by considering total free energy $\Delta\Delta G^\circ_{U\rightarrow N}$ for the two-state mutants and the individual free energy values, $\Delta\Delta G^\circ_{U\rightarrow I}$ or $\Delta\Delta G^\circ_{I\rightarrow N}$, for the three-state mutants, we find a heterogeneous distribution of residues with no specific hydrophobicity trend apparent in the analysis (Figure S5). On the basis of our previous study,[22] we know that the U → I transition of the three-state mutants is a true indicator of the global folding process. However, the $\Delta\Delta G^\circ_{U\rightarrow I}$ also does not correlate well with the empirical parameters describing the ASA change (Figure S6A). This particular result appears to be a consequence of the destabilizing effect of the terminal His in comparison to the native Phe. Another interesting aspect that emerges from this comparison is that

DOI: 10.1021/acs.biochem.8b00805
Biochemistry 2018, 57, 6669–6678

Ser at the penultimate residue stabilizes PagP irrespective of the terminal residue (Phe or His). In line with our previous analysis of PagP,[22] we believe that the stabilizing packing interactions established by the Ser side chain might be the reason for such high stability demonstrated by PagP-SH.

Analysis of the folded PagP-X^{160}H mutants via cold SDS−PAGE also reveals that several mutants exhibit varied percents of dimers (Figure S7). To verify if the observed dimerization is indeed due to the mutation at the penultimate position and is not an experimental artifact, we calculated the DPR utilized for our folding experiments. Considering an aggregation number of ∼55−60 DPC molecules in one micelle,[43] at our experimental DPR of 3300:1, we obtain ∼50 micelles for one molecule of protein. Hence, we conclude that the ability of some PagP-X^{160}H variants to dimerize is intrinsic to the mutant. We also find that residues with small or polar side chains (such as Ser and Thr) exhibit the anticipated mobility shift upon folding, whereas residues with either hydrophobic or hydrophilic side chains fail to demonstrate the electrophoretic mobility shift upon folding. As with the nonpolar ASA, there is poor correlation between the fraction of the mutant migrating as a monomer/dimer and the normalized folding free energy of the residue substituted at the interface (Figure S6B). In addition, we obtain only a qualitative propensity of PagP-XH mutants bearing hydrophilic residues at the penultimate position to form dimers in cold SDS−PAGE gels. Effectively, the dimerization ability of PagP does not show any specific trend when compared with the residue type of the mutation at the penultimate position (discussed in detail in the following section; also see Figure 4). The best correlation we obtain for the $\Delta\Delta G^\circ$ is with the nonpolar ASA change. We also find that the penultimate residue influences the balance between high stability and a smooth folding landscape that is devoid of observable intermediates in the folding pathway.

The Structural Compactness of the PagP Barrel Dictates the Interaction Energy between Terminal and Penultimate Residues. Our observation that the $\Delta\Delta G^\circ$ for the PagP-XH mutants differs from known free energy scales indicates a strong influence of the terminal His on the structure and folding of PagP. We have observed in our earlier study[22] that the penultimate residue (X^{160}) influences the thermodynamic contribution of the terminal residue (X^{161}). In an effort to understand the interaction energetics between the terminal and penultimate residues, we performed a double-mutant cycle analysis using wild-type PagP (PagP-$Q^{160}F^{161}$) as the reference and previously reported free energy values of PagP-$X^{160}F^{161}$.[22] We used $\Delta G^\circ_{U\rightarrow N}$ for the two-state mutants and $\Delta G^\circ_{U\rightarrow I}$ for the three-state mutants and generated the double-mutant cycle chart (Figure 3). Interestingly, we find that a majority of residues show a negative ΔG_{int}, indicating that the interaction between these residues is favorable. The highest ΔG_{int} is seen for hydrophobic residues with bulky side chains (Leu, −8.5 ± 0.91 kcal mol^{-1}; Trp, −7.2 ± 0.91 kcal mol^{-1}; Phe, −5.8 ± 0.91 kcal mol^{-1}). Residues with polar or small apolar side chains displayed interaction energies close to zero, suggesting little or no interaction between the coupled residues. Along similar lines, we performed the double-mutant cycle analysis using the overall free energy ($\Delta G^\circ_{U\rightarrow N}$) for all mutants (Figure S8). We find that although the magnitude of coupling energies has decreased for the mutants displaying three-state profiles, hydrophobic residues (including Leu, Ile, and Val) do exhibit negative ΔG_{int} values.

As is the case with several OMPs, the folded and unfolded states of PagP differ in their electrophoretic mobilities.[34,35] We utilized this property to assess the folded state of the PagP-X^{160}H mutant library and to check if His incorporation caused structural alterations in the barrel (Figure S7). We find that only residues with small or polar side chains (Ser, Gln, Ala, Thr, and Gly) possessing ΔG_{int} values ranging from −2 to 2 kcal mol^{-1} exhibit the anticipated mobility shift upon folding, comparable to that of PagP-WT. In contrast, residues at the extreme ends of the ΔG° plot (see Figure 1C) and unusually high ΔG_{int} values do not exhibit an electrophoretic mobility shift upon folding (Figure 4). We performed a similar comparison of the electrophoretic mobilities of the mutants with the interaction energies derived using the overall free energy ($\Delta G^\circ_{U\rightarrow N}$) of all mutants, irrespective of whether they show two-state or three-state folding profiles (Figure S9). Furthermore, the correlation of ΔG_{int} (shown in Figure 3) with other empirical side chain parameters or the PagP dimerization propensity is not statistically significant (Figure S10). We

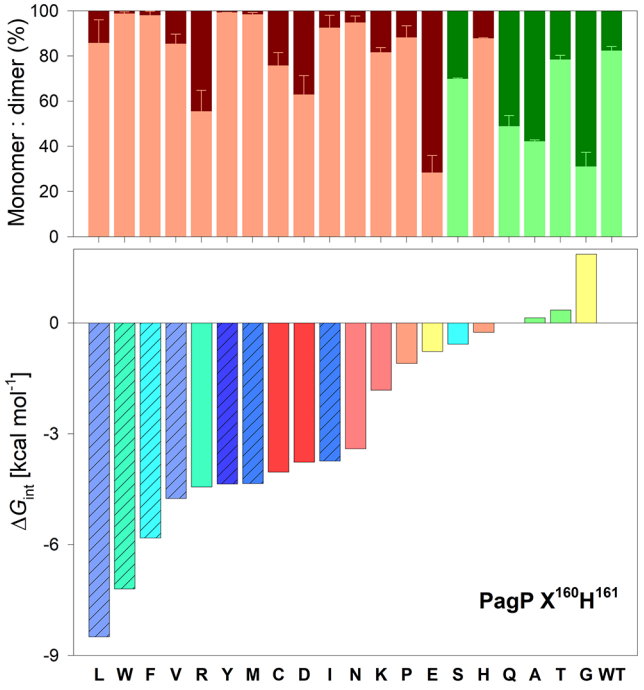

Figure 4. PagP-$X^{160}H^{161}$ interaction energy profile that correlates well with the electrophoretic mobility. The electrophoretic mobility and dimer population (top) are compared with the ΔG_{int} values (bottom) (see Figure S9 for the ΔG_{int} calculation using $\Delta G^\circ_{U\rightarrow N}$). In the top panel, mutants showing the anticipated mobility shift upon folding on cold SDS−PAGE gels, similar to PagP-WT, are colored green. Mutants lacking the electrophoretic mobility are shown as brown histograms. The percent population of PagP migrating as a monomer and dimer is depicted as light and dark fills in the histogram, respectively. Error bars represent the standard deviation derived from two independent experiments. In the bottom panel, the ΔG_{int} values between the terminal (X^{160}) and penultimate (F^{161}) residues computed for all 20 residues and normalized with respect to alanine are shown. The color code and histogram representation are retained from Figure 1. Mutants with lower ΔG_{int} values (bottom, right side) also exhibit proper gel mobilities (top, green histograms). On the other hand, mutants that do not show the expected mobility shift display higher interaction energies. A direct correlation between the dimer population and energetic parameters was not seen.

DOI: 10.1021/acs.biochem.8b00805
Biochemistry 2018, 57, 6669−6678

further verified that PagP mutants lacking electrophoretic mobility are indeed folded using the protease protection assay (see Figure S7). We also computed the $\langle\lambda\rangle$ values for fully folded and fully unfolded samples and compared them across mutants demonstrating differing patterns of mobility shift and dimerization on SDS−PAGE (Figure S11). They were found to be quite similar across all mutants (averaging to ∼357.6 nm for folded samples and ∼362.6 nm for unfolded samples), suggesting that all the mutants are indeed folded. Hence, the difference in the electrophoretic mobility of OMPs arises from structural compaction of the folded state compared to the unfolded state.[22,35] Therefore, the influence of His at the lipid-facing interface on the tertiary structure of PagP depends on the penultimate residue in the sequence.

Next, we performed spectroscopic analysis using far-UV CD at 215 nm (θ_{215}) and 231 nm (θ_{231}) to verify if the PagP structure is perturbed by the incorporation of histidine at the C-terminus (Figure 5). Because of β-rich structure, the far-UV CD spectrum of PagP displays a negative trough centered at 215 nm. Additionally, structural compaction of PagP can be assessed using a unique positive CD centered at 231 nm, which arises from tertiary interactions formed between Y^{26} and W^{66} in the folded barrel.[44] The molecular basis of this CD exciton couplet has been studied in detail previously.[40,45] We find that the folded PagP-X^{160}H mutants exhibit a marginal variation in the secondary structure content (−40 to −30 mdeg). More importantly, the θ_{231} value, which is a reliable indicator of tertiary packing, also carries significant variation across mutants ranging from approximately 8 mdeg (strong tertiary interaction) for PagP-QH to approximately −3 mdeg (poor tertiary interactions and loss of barrel compaction) for PagP-LH. One must note here that while the tertiary packing (strong or poor) can be inferred directly from the strength of the θ_{231} signal, the reverse might not always be true. For example, the specific geometry of the aromatic interaction between Y^{26} and W^{66} that gives rise to the θ_{231} signal could be abolished without severely affecting the overall stability of the barrel. In our study of the PagP-$X^{160}H^{161}$ mutant library, the correlation that we establish between the θ_{231} value and tertiary packing has been consolidated by evidence from electrophoretic mobility experiments (see Figure 4).

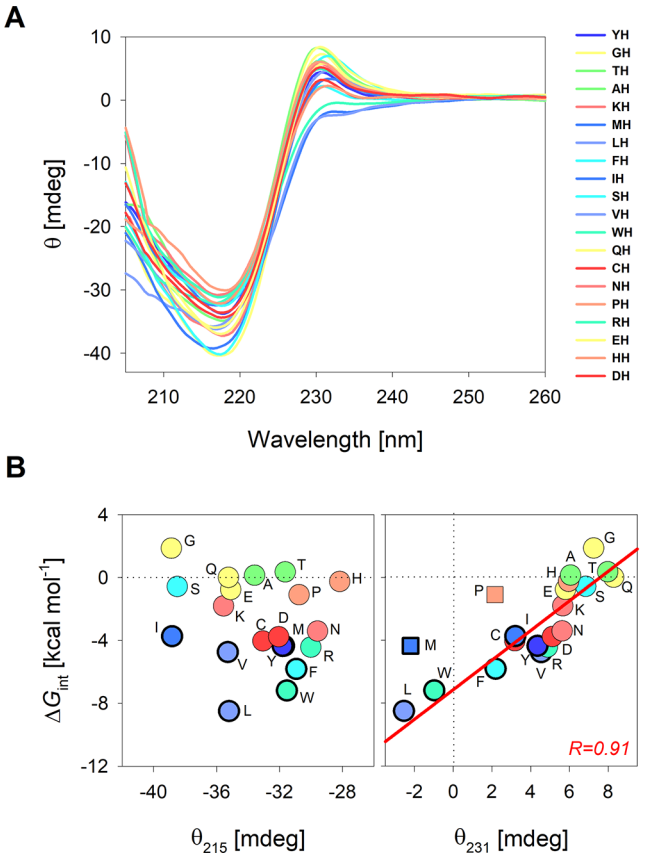

Figure 5. Strong correlation of the interaction energy profile with the tertiary interactions in the folded PagP-$X^{160}H^{161}$ scaffold. (A) Far-UV CD wavelength scans recorded to examine the secondary structure content (negative maximum at ∼215 nm) and tertiary aromatic interactions established upon barrel assembly (positive maximum at ∼231 nm) for all mutants from the PagP-$X^{160}H^{161}$ library. Single-letter codes ($X^{160}H^{161}$) are used for the mutants, and the color code is retained from Figure 1. (B) Correlation plots for the secondary structure content (θ_{215}, left) and the tertiary interaction (θ_{231}, right) with the interaction energy (ΔG_{int}) for the PagP-$X^{160}H^{161}$ mutants. Variants displaying three-state profiles, for which $\Delta G^{\circ}_{U\rightarrow I}$ has been used to compute the interaction energy, are shown as symbols with thicker edges. We find a strong correlation of the interaction energies with θ_{231} (in the right panel, the solid red line shows the linear fit to the correlation). Points excluded from the fit are shown as squares.

Comparisons of the folding free energy or the m value and the change in ASA with the change in θ_{215} or θ_{231} do not yield any significant correlations (Figures S12 and S13). However, we reasoned that the abnormally large values of ΔG_{int} and the lack of electrophoretic mobility for the hydrophobic residue mutants must correlate with structural abnormality in the PagP barrel. Indeed, when we mapped the ΔG_{int} with the far-UV (θ_{215}) and near-UV (θ_{231}) CD ellipticity values, we found a strong inverse correlation (R = 0.91) between the ΔG_{int} and θ_{231} CD values (Figure 5B). Hydrophobic residues such Leu and Val, with high coupling energy values, exhibit poor tertiary packing, whereas polar or small apolar residues, such as Ser and Gly, demonstrate higher tertiary CD values (θ_{231}). We find that placing a hydrophobic residue or strongly hydrophilic residue at the penultimate position disrupts the molecular interaction network in the vicinity of X^{160}. This is reflected in the decrease in the tertiary exciton CD values (θ_{231}) as well as the loss of the electrophoretic mobility shift of these mutants. In cases in which the substituted residue is hydrophobic in nature (Leu, for example, showing a ΔG_{int} value of −8.5 ± 0.91 kcal mol^{-1}), a coupling interaction involving the side chain as well as the backbone atoms is established between residues 160 and 161. The bulky side chain of L^{160} could indirectly influence H^{161} by occluding the space available for nearby atoms to interact with its side chain, whereas the backbone torsion angle of L^{160} could directly affect the side chain orientation of H^{161}. This interaction appears to salvage the overall free energy of the molecule, possibly by formation of a stable intermediate. On the other hand, when we substitute a strongly hydrophilic residue at X^{160} (Asp, for example, with a ΔG_{int} value of −3.8 ± 0.9 kcal mol^{-1}), it is unable to establish a strong coupling interaction network and, consequently, the free energy observed for PagP-D^{160} is lower than that of wild-type PagP. In contrast to both these conditions, when we introduce a polar residue with hydrogen bonding ability or a small apolar residue with a modest side chain ASA, the molecular interaction network around X^{160} is largely unperturbed and, therefore, no loss of tertiary CD or electrophoretic mobility is observed. By extension, no coupling energy is observed between the terminal two residues, when polar or small apolar

DOI: 10.1021/acs.biochem.8b00805
Biochemistry 2018, 57, 6669−6678

residues, such as Ser and Gly, are present at the penultimate position, as there is no significant local destabilization. Therefore, a strong coupling interaction between residues sequentially adjacent at the membrane interface is compensating for a structural defect in the barrel packing.

DISCUSSION

The thermodynamic contribution of the aromatic side chain of histidine at the water−lipid interface of the eight-stranded barrel PagP is unfavorable. In comparison with the hydrophobic side chain of phenylalanine that is natively present, we obtain a destabilization of ∼4.0 kcal mol^{-1} due to the C-terminal interface histidine. At the water−lipid interface position of PagP-X^{161}, we had previously derived an ASP (atomic solvation parameter) value of 0.043 ± 0.01 kcal mol^{-1} Å^{-2}.[22] This value is higher than the ASP derived for the Wimley−White interface scale (∼0.0131 kcal mol^{-1} Å^{-2}).[41] We had previously reasoned that the abnormally large ASP could be due to changes in the ASA (m value) that are magnified in DPC micelles.[22] Another reason for this observation could be that while the denatured state ensemble achieved by PagP variants may be identical, the folded state could retain varying degrees of structure and thereby affect the magnitude of free energy changes observed upon folding (as evidenced by the far-UV CD spectra in Figure 5A). The destabilization due to the F^{161} → H substitution is therefore magnified in our measurements. While the absolute $\Delta G°$ values are overestimated, we conclude from the correlation of numerical values in partitioning energetics that thermodynamic exclusion could be one of the critical reasons for histidine not occurring frequently in the C-terminal water−lipid interface regions of membrane proteins. Furthermore, the β-signal sequence is known to be associated *in vivo* with initiation of the membrane insertion and folding of the OMP substrate through interaction with the β-barrel assembly machinery (BAM) complex.[23,46,47] While we do not have evidence of whether His is evolutionarily unfavored for OMP−BAM interaction, the final part of the assembly process, namely the folding and stabilization in the membrane, would still depend on the inherent properties of the β-signal residues and their interactions with the membrane interface. It is also likely that thermodynamics of barrel−BAM interaction may be independent of barrel thermodynamics itself after dissociation of the barrel from the BAM complex. The destabilization by an interface histidine may be offset in the asymmetric bacterial outer membrane, the inner leaflet of which contains a significant fraction of zwitterionic or negatively charged lipid headgroups.[48] Histidine, which is also known to function as a pH sensor, might play a crucial role as an interface residue and contribute to regulating the physiological pH of the periplasmic microenvironment.[49] Hence, the evolutionary retention of an interface histidine in OMP sequences could have likely arisen from functional requirements.

Data from the PagP-X^{160}H mutant library reiterate the importance of polar side chains present in the interior of membrane proteins[50] and their role in thermodynamic stabilization. Indeed, the nature of the penultimate residue (Q^{160} in wild-type PagP) dictates the folding behavior of this protein. We find that although the incorporation of a hydrophobic residue at position 160 increases the overall $\Delta G°$ in DPC micelles, it affects the folding pathway of PagP and populates an intermediate. Furthermore, an earlier study of the folding pathway of PagP[20] suggested that Q^{160} may be part of the PagP folding nucleus. It points out that Q^{160} possesses a high ϕ value and therefore appears to be well structured in the transition state ensemble. Q^{160} is also involved in the formation of a hydrogen bond with W^{60}. This side chain-driven hydrogen bonding prevalent in the interior of the PagP barrel is crucial to the formation of the folded structure. The double-mutant cycle analysis (Figure 4) shows that the interaction energy is minimal when the residue possesses a polar or small apolar side chain. Our analysis suggests that the coupling energy between the terminal and penultimate residues is highest when the inherent destabilization due to weaker tertiary packing is also maximal. We have observed in our earlier study[22] that the destabilizing effect at the C-terminal residue can be salvaged (in part) by interactions formed by the penultimate residue. Whether the high ΔG_{int} is a cause or consequence of poor structural compaction is presently open to further exploration. However, we also note that previous reports on double-mutant cycle analysis, for either water-soluble[33,51,52] or membrane proteins,[19] have focused on alanine mutations to characterize the interaction between a pair of residues. This is one of the few studies to analyze the ΔG_{int} of not-to-alanine mutants. Interpretation of not-to-alanine double-mutant cycles must therefore be conducted with caution.[53] Furthermore, interaction energies are generally analyzed between residues that are separated in sequence but are spatially proximal,[33] whereas we have evaluated the coupling interactions between side chains of residues that are adjacent in sequence.

CONCLUSION

Our findings using PagP as our model protein are in good agreement with a previous observation that hydrophobicity, and not aromaticity, is the driving factor behind stabilization at the C-terminal interface of OMPs.[22] Such a conclusion is in contrast to popular interface scales,[41,54] which warrant the requirement of a residue with amphiphilic characteristics at the water−lipid interface. As the energetics of the terminal and penultimate residues are coupled in our PagP-X^{160}H^{161} mutants, a deviation in free energy values from well-established hydrophobicity scales is not surprising. Moreover, it has also been observed that protein-specific constraints can dictate which chemical property (polar nature or hydrophobic nature) of such amphiphilic molecules will aid in thermodynamic stabilization.[55] Under our experimental conditions, the His side chain is not expected to undergo ionization and, therefore, the aromatic character (albeit lower than that of the aromatic triplet of Phe, Tyr and Trp) of its side chain would be a significant contributor to the measured energetics. Our thermodynamic analysis, although limited to micellar systems, suggests that the aromaticity, the bulky size of the side chain, and the hydrophobicity are more significant contributors than polarity and H-bonding ability to favorable partitioning of aromatic amino acids to the membrane interface. Similar observations have been made from studies of indoles and indole analogues[56−58] as well as transmembrane α-helices[37] that examine the preference of Trp at the water−membrane interface.

In conclusion, our biophysical analysis of the PagP-X^{160}H^{161} library reveals a thermodynamic basis for how interface histidine residues affect the folding pathway of a model OMP. Histidine can also influence scaffold compaction by promoting the formation of non-native interactions that affect the observed energetics of the protein. The OMP primary sequence has evolved to balance both folding (by the BAM

DOI: 10.1021/acs.biochem.8b00805
Biochemistry 2018, 57, 6669−6678

complex) and thermodynamic and kinetic stability of the folded protein scaffold. We conclude that the evolutionary selection of an interface histidine would be strongly driven by functional importance rather than by protein energetics. Interesting observations made from the analysis of the model transmembrane β-barrel PagP as well as the approaches to investigating membrane protein folding outlined in this study could pave the way for a better understanding of residue-dependent physical factors that govern the folding and stability of membrane proteins.

■ ASSOCIATED CONTENT

Supporting Information

The Supporting Information is available free of charge on the ACS Publications website at DOI: 10.1021/acs.biochem.8b00805.

Additional figures, table, and supporting data (PDF)

■ AUTHOR INFORMATION

Corresponding Author

*Molecular Biophysics Laboratory, Department of Biological Sciences, Indian Institute of Science Education and Research, Room 324, III Floor, Block C, Academic Building 3, Bhauri, Bhopal 462066, India. E-mail: maha@iiserb.ac.in. Phone: +91-755-2691423. Fax: +91-755-2692392.

ORCID

Radhakrishnan Mahalakshmi: 0000-0003-1549-7550

Author Contributions

P.V.V., H.N., and P.Z. contributed equally to this work. R.M. designed the research. B.R.I., P.V.V., H.N., and P.Z. performed the research. B.R.I., P.Z., and R.M. analyzed the data. R.M. wrote the paper with input from B.R.I. and P.Z. All the authors have given approval to the manuscript.

Funding

B.R.I. thanks the University Grants Commission, Government of India, for a senior research fellowship. R.M. is a Wellcome Trust/DBT India Alliance Intermediate Fellow. This work was supported by funds from Science and Engineering Research Board Grants EMR/2016/001774 and SB/WEA-13/2016 and Wellcome Trust/DBT India Alliance Grant IA/I/14/1/501305 to R.M.

Notes

The authors declare no competing financial interest.

■ ABBREVIATIONS

BAM, β-barrel assembly machinery; CD, circular dichroism; C_m, midpoint of chemical denaturation; DPC, *n*-dodecylphosphocholine; DPR, detergent-to-protein ratio; ΔG°_F, Gibbs folding free energy; GdnHCl, guanidine hydrochloride; *m* value, change in the accessible surface area upon protein unfolding; OMP, outer membrane protein; PagP, PhoPQ-activated gene P; PK, proteinase K; WT, wild-type.

■ REFERENCES

(1) Loewenthal, R., Sancho, J., and Fersht, A. R. (1992) Histidine-aromatic interactions in barnase. Elevation of histidine pKa and contribution to protein stability. *J. Mol. Biol. 224*, 759−770.

(2) Cauet, E., Rooman, M., Wintjens, R., Lievin, J., and Biot, C. (2005) Histidine-Aromatic Interactions in Proteins and Protein-Ligand Complexes: Quantum Chemical Study of X-ray and Model Structures. *J. Chem. Theory Comput. 1*, 472−483.

(3) Jasanoff, A., and Weiss, M. A. (1993) Aromatic-histidine interactions in the zinc finger motif: structural inequivalence of phenylalanine and tyrosine in the hydrophobic core. *Biochemistry 32*, 1423−1432.

(4) Fernandez-Recio, J., Vazquez, A., Civera, C., Sevilla, P., and Sancho, J. (1997) The tryptophan/histidine interaction in alpha-helices. *J. Mol. Biol. 267*, 184−197.

(5) Bhattacharyya, R., Saha, R. P., Samanta, U., and Chakrabarti, P. (2003) Geometry of interaction of the histidine ring with other planar and basic residues. *J. Proteome Res. 2*, 255−263.

(6) Makwana, K. M., Raghothama, S., and Mahalakshmi, R. (2013) Stabilizing effect of electrostatic vs. aromatic interactions in diproline nucleated peptide beta-hairpins. *Phys. Chem. Chem. Phys. 15*, 15321−15324.

(7) Ulmschneider, M. B., and Sansom, M. S. (2001) Amino acid distributions in integral membrane protein structures. *Biochim. Biophys. Acta, Biomembr. 1512*, 1−14.

(8) Ulmschneider, M. B., Sansom, M. S., and Di Nola, A. (2005) Properties of integral membrane protein structures: derivation of an implicit membrane potential. *Proteins: Struct., Funct., Genet. 59*, 252−265.

(9) Killian, J. A., and von Heijne, G. (2000) How proteins adapt to a membrane-water interface. *Trends Biochem. Sci. 25*, 429−434.

(10) Fairman, J. W., Noinaj, N., and Buchanan, S. K. (2011) The structural biology of beta-barrel membrane proteins: a summary of recent reports. *Curr. Opin. Struct. Biol. 21*, 523−531.

(11) Lee, S. A., Eyeson, R., Cheever, M. L., Geng, J., Verkhusha, V. V., Burd, C., Overduin, M., and Kutateladze, T. G. (2005) Targeting of the FYVE domain to endosomal membranes is regulated by a histidine switch. *Proc. Natl. Acad. Sci. U. S. A. 102*, 13052−13057.

(12) Kampmann, T., Mueller, D. S., Mark, A. E., Young, P. R., and Kobe, B. (2006) The Role of histidine residues in low-pH-mediated viral membrane fusion. *Structure 14*, 1481−1487.

(13) Bustad, H. J., Skjaerven, L., Ying, M., Halskau, O., Baumann, A., Rodriguez-Larrea, D., Costas, M., Underhaug, J., Sanchez-Ruiz, J. M., and Martinez, A. (2012) The peripheral binding of 14−3-3gamma to membranes involves isoform-specific histidine residues. *PLoS One 7*, No. e49671.

(14) Martfeld, A. N., Greathouse, D. V., and Koeppe, R. E., 2nd (2016) Ionization Properties of Histidine Residues in the Lipid Bilayer Membrane Environment. *J. Biol. Chem. 291*, 19146−19156.

(15) Wimley, W. C., Creamer, T. P., and White, S. H. (1996) Solvation energies of amino acid side chains and backbone in a family of host-guest pentapeptides. *Biochemistry 35*, 5109−5124.

(16) Hessa, T., Kim, H., Bihlmaier, K., Lundin, C., Boekel, J., Andersson, H., Nilsson, I., White, S. H., and von Heijne, G. (2005) Recognition of transmembrane helices by the endoplasmic reticulum translocon. *Nature 433*, 377−381.

(17) Moon, C. P., and Fleming, K. G. (2011) Side-chain hydrophobicity scale derived from transmembrane protein folding into lipid bilayers. *Proc. Natl. Acad. Sci. U. S. A. 108*, 10174−10177.

(18) Lin, M., Gessmann, D., Naveed, H., and Liang, J. (2016) Outer Membrane Protein Folding and Topology from a Computational Transfer Free Energy Scale. *J. Am. Chem. Soc. 138*, 2592−2601.

(19) Hong, H., Park, S., Flores Jiménez, R. H., Rinehart, D., and Tamm, L. K. (2007) Role of aromatic side chains in the folding and thermodynamic stability of integral membrane proteins. *J. Am. Chem. Soc. 129*, 8320−8327.

(20) Huysmans, G. H., Baldwin, S. A., Brockwell, D. J., and Radford, S. E. (2010) The transition state for folding of an outer membrane protein. *Proc. Natl. Acad. Sci. U. S. A. 107*, 4099−4104.

(21) Marx, D. C., and Fleming, K. G. (2017) Influence of Protein Scaffold on Side-Chain Transfer Free Energies. *Biophys. J. 113*, 597−604.

(22) Iyer, B. R., Zadafiya, P., Vetal, P. V., and Mahalakshmi, R. (2017) Energetics of side-chain partitioning of beta-signal residues in unassisted folding of a transmembrane beta-barrel protein. *J. Biol. Chem. 292*, 12351−12365.

DOI: 10.1021/acs.biochem.8b00805
Biochemistry 2018, 57, 6669−6678

(23) Robert, V., Volokhina, E. B., Senf, F., Bos, M. P., Van Gelder, P., and Tommassen, J. (2006) Assembly factor Omp85 recognizes its outer membrane protein substrates by a species-specific C-terminal motif. *PLoS Biol. 4*, No. e377.
(24) Struyve, M., Moons, M., and Tommassen, J. (1991) Carboxy-terminal phenylalanine is essential for the correct assembly of a bacterial outer membrane protein. *J. Mol. Biol. 218*, 141−148.
(25) de Cock, H., Struyve, M., Kleerebezem, M., van der Krift, T., and Tommassen, J. (1997) Role of the carboxy-terminal phenylalanine in the biogenesis of outer membrane protein PhoE of Escherichia coli K-12. *J. Mol. Biol. 269*, 473−478.
(26) Bishop, R. E. (2005) The lipid A palmitoyltransferase PagP: molecular mechanisms and role in bacterial pathogenesis. *Mol. Microbiol. 57*, 900−912.
(27) Lehr, U., Schutz, M., Oberhettinger, P., Ruiz-Perez, F., Donald, J. W., Palmer, T., Linke, D., Henderson, I. R., and Autenrieth, I. B. (2010) C-terminal amino acid residues of the trimeric autotransporter adhesin YadA of Yersinia enterocolitica are decisive for its recognition and assembly by BamA. *Mol. Microbiol. 78*, 932−946.
(28) Paramasivam, N., Habeck, M., and Linke, D. (2012) Is the C-terminal insertional signal in Gram-negative bacterial outer membrane proteins species-specific or not? *BMC Genomics 13*, 510.
(29) Kleinschmidt, J. H. (2006) Folding kinetics of the outer membrane proteins OmpA and FomA into phospholipid bilayers. *Chem. Phys. Lipids 141*, 30−47.
(30) Kleinschmidt, J. H. (2015) Folding of beta-barrel membrane proteins in lipid bilayers - Unassisted and assisted folding and insertion. *Biochim. Biophys. Acta, Biomembr. 1848*, 1927−1943.
(31) Dubey, A. A., Singh, M. I., and Jain, V. (2016) Rapid and Robust PCR-Based All-Recombinant Cloning Methodology. *PLoS One 11*, No. e0152106.
(32) Santoro, M. M., and Bolen, D. W. (1992) A test of the linear extrapolation of unfolding free energy changes over an extended denaturant concentration range. *Biochemistry 31*, 4901−4907.
(33) Horovitz, A. (1996) Double-mutant cycles: a powerful tool for analyzing protein structure and function. *Folding Des. 1*, R121−126.
(34) Iyer, B. R., and Mahalakshmi, R. (2015) Residue-Dependent Thermodynamic Cost and Barrel Plasticity Balances Activity in the PhoPQ-Activated Enzyme PagP of Salmonella typhimurium. *Biochemistry 54*, 5712−5722.
(35) Burgess, N. K., Dao, T. P., Stanley, A. M., and Fleming, K. G. (2008) Beta-barrel proteins that reside in the Escherichia coli outer membrane in vivo demonstrate varied folding behavior in vitro. *J. Biol. Chem. 283*, 26748−26758.
(36) Hwang, P. M., Choy, W. Y., Lo, E. I., Chen, L., Forman-Kay, J. D., Raetz, C. R., Prive, G. G., Bishop, R. E., and Kay, L. E. (2002) Solution structure and dynamics of the outer membrane enzyme PagP by NMR. *Proc. Natl. Acad. Sci. U. S. A. 99*, 13560−13565.
(37) Situ, A. J., Kang, S. M., Frey, B. B., An, W., Kim, C., and Ulmer, T. S. (2018) Membrane Anchoring of alpha-Helical Proteins: Role of Tryptophan. *J. Phys. Chem. B 122*, 1185−1194.
(38) *PyMOL Molecular Graphics System*, version 2.0, Schrödinger, LLC.
(39) Miller, S., Janin, J., Lesk, A. M., and Chothia, C. (1987) Interior and surface of monomeric proteins. *J. Mol. Biol. 196*, 641−656.
(40) Khan, M. A., Moktar, J., Mott, P. J., and Bishop, R. E. (2010) A thiolate anion buried within the hydrocarbon ruler perturbs PagP lipid acyl chain selection. *Biochemistry 49*, 2368−2379.
(41) Wimley, W. C., and White, S. H. (1996) Experimentally determined hydrophobicity scale for proteins at membrane interfaces. *Nat. Struct. Mol. Biol. 3*, 842−848.
(42) Chothia, C. (1976) The nature of the accessible and buried surfaces in proteins. *J. Mol. Biol. 105*, 1−12.
(43) Lazaridis, T., Mallik, B., and Chen, Y. (2005) Implicit solvent simulations of DPC micelle formation. *J. Phys. Chem. B 109*, 15098−15106.
(44) Adil Khan, M., Neale, C., Michaux, C., Pomes, R., Prive, G. G., Woody, R. W., and Bishop, R. E. (2007) Gauging a hydrocarbon ruler by an intrinsic exciton probe. *Biochemistry 46*, 4565−4579.
(45) Leney, A. C., McMorran, L. M., Radford, S. E., and Ashcroft, A. E. (2012) Amphipathic polymers enable the study of functional membrane proteins in the gas phase. *Anal. Chem. 84*, 9841−9847.
(46) Gessmann, D., Chung, Y. H., Danoff, E. J., Plummer, A. M., Sandlin, C. W., Zaccai, N. R., and Fleming, K. G. (2014) Outer membrane beta-barrel protein folding is physically controlled by periplasmic lipid head groups and BamA. *Proc. Natl. Acad. Sci. U. S. A. 111*, 5878−5883.
(47) Lee, J., Xue, M., Wzorek, J. S., Wu, T., Grabowicz, M., Gronenberg, L. S., Sutterlin, H. A., Davis, R. M., Ruiz, N., Silhavy, T. J., and Kahne, D. E. (2016) Characterization of a stalled complex on the beta-barrel assembly machine. *Proc. Natl. Acad. Sci. U. S. A. 113*, 8717−8722.
(48) Abellon-Ruiz, J., Kaptan, S. S., Basle, A., Claudi, B., Bumann, D., Kleinekathofer, U., and van den Berg, B. (2017) Structural basis for maintenance of bacterial outer membrane lipid asymmetry. *Nat. Microbiol. 2*, 1616−1623.
(49) Krulwich, T. A., Sachs, G., and Padan, E. (2011) Molecular aspects of bacterial pH sensing and homeostasis. *Nat. Rev. Microbiol. 9*, 330−343.
(50) Jayasinghe, S., Hristova, K., and White, S. H. (2001) Energetics, stability, and prediction of transmembrane helices. *J. Mol. Biol. 312*, 927−934.
(51) Cockroft, S. L., and Hunter, C. A. (2007) Chemical double-mutant cycles: dissecting non-covalent interactions. *Chem. Soc. Rev. 36*, 172−188.
(52) Sokolovski, M., Cveticanin, J., Hayoun, D., Korobko, I., Sharon, M., and Horovitz, A. (2017) Measuring inter-protein pairwise interaction energies from a single native mass spectrum by double-mutant cycle analysis. *Nat. Commun. 8*, 212.
(53) Faiman, G. A., and Horovitz, A. (1996) On the choice of reference mutant states in the application of the double-mutant cycle method. *Protein Eng., Des. Sel. 9*, 315−316.
(54) Hessa, T., Meindl-Beinker, N. M., Bernsel, A., Kim, H., Sato, Y., Lerch-Bader, M., Nilsson, I., White, S. H., and von Heijne, G. (2007) Molecular code for transmembrane-helix recognition by the Sec61 translocon. *Nature 450*, 1026−1030.
(55) Yuen, C. T., Davidson, A. R., and Deber, C. M. (2000) Role of aromatic residues at the lipid-water interface in micelle-bound bacteriophage M13 major coat protein. *Biochemistry 39*, 16155−16162.
(56) Gaede, H. C., Yau, W. M., and Gawrisch, K. (2005) Electrostatic contributions to indole-lipid interactions. *J. Phys. Chem. B 109*, 13014−13023.
(57) Persson, S., Antoinette Killian, J., and Lindblom, G. (1998) Molecular ordering of interfacially localized tryptophan analogs in ester- and ether-lipid bilayers studied by 2H-NMR. *Biophys. J. 75*, 1365−1371.
(58) de Jesus, A. J., and Allen, T. W. (2013) The role of tryptophan side chains in membrane protein anchoring and hydrophobic mismatch. *Biochim. Biophys. Acta, Biomembr. 1828*, 864−876.

DOI: 10.1021/acs.biochem.8b00805
Biochemistry 2018, 57, 6669−6678